Article

A Comprehensive Energy Model for an Optimal Design of a Hybrid Refrigerated Van

Angelo Maiorino [1,*], Adrián Mota-Babiloni [2], Fabio Petruzziello [1], Manuel Gesù Del Duca [1], Andrea Ariano [1] and Ciro Aprea [1]

[1] Department of Industrial Engineering, University of Salerno, Via Giovanni Paolo II 132, 84084 Fisciano, SA, Italy; fpetruzziello@unisa.it (F.P.); mdelduca@unisa.it (M.G.D.D.); aariano94@gmail.com (A.A.); aprea@unisa.it (C.A.)

[2] ISTENER Research Group, Department of Mechanical Engineering and Construction, Campus de Riu Sec s/n, Universitat Jaume I, E-12071 Castelló de la Plana, Spain; mota@uji.es

* Correspondence: amaiorino@unisa.it; Tel.: +39-(0)-89-964-105

Abstract: The path towards decarbonization requires a progressive adaptation of all refrigeration systems, but only stationary ones have been intensely studied to improve their environmental performance. However, refrigerated transport is vital in the cold chain and must be considered in the green transition. In this paper, we propose a model for a hybrid refrigerated van that includes photovoltaic panels and electric batteries to decrease total greenhouse gas emissions from the engine. Thermal, electrical, and battery sub-models are considered and integrated into the comprehensive hybrid solar-powered refrigerated van model. Different technologies are compared, including lithium and lead-acid batteries and three different types of photovoltaic panels. The model was validated regarding van fuel consumption, showing a 4% deviation. Single and multiple delivery scenarios are considered to assess the energy, economic, and environmental benefits. Monthly CO_2,e emissions could be reduced by 20% compared to a standard refrigerated van. Despite the environmental benefits provided by this sustainable solution, the payback period is still too long (above 20 years) because of the necessary investment to adapt the vehicle and considering fuel and electricity prices currently.

Keywords: refrigerated transport; photovoltaic panels; electrical batteries; thermal model; cold chain; carbon emissions

1. Introduction

The transport sector requires effective public interventions and measures to reduce CO_2,e (carbon dioxide equivalent) emissions and reduce vulnerability to climate change. CO_2,e emissions from this sector are about 30% in developed countries of anthropogenic origin and 23% worldwide [1]. There are 4 million refrigerated road vehicles, and together with refrigerated containers and supermarkets, 45% of the electricity is consumed by refrigeration equipment [2]. Of that, 55% of the refrigerated road vehicles are vans, followed by semi-trailers and trucks (25% and 20%, respectively). CO_2,e emissions per kg of food and kilometer from refrigeration systems of the small vehicles are more than double the larger ones, for both chilled and frozen distribution of different products [3]. More than 98% of all foods within the UK are transported by road, and the distances traveled have increased in recent years [4]. Tertiary distribution using rigid vehicles was the most energy-intensive transportation method, while primary distribution at ambient temperature was the least.

Refrigerated transportation, which is more intensive than stationary refrigerated systems, has also increased in recent years. Overall CO_2 emissions of vans with refrigeration units are 15% higher than standard vehicles, with NO_X emissions estimated to rise by 18%. The weight of the additional engine in the transport refrigerated sector is significant [5]. Sovacool et al. [6] highlighted the transport and delivery sector as one of the most carbon-intensive emissions of the food and beverages industry. A significant improvement was

the uptake of distributed generation and small-scale renewable energy systems. It is one of the three most significant areas with higher energy and carbon savings potential.

Compared to other refrigeration systems, refrigerated transport has not focused on transitioning to lower-environmental-impact refrigerants [7]. Li [8] determined a theoretical reduction in CO_2,e emissions between 5% and 15% in a refrigerated trailer when replacing R404A with R452A. Citarella et al. [9] conducted a thermo-economic and environmental analysis in which R452A presented low set-up costs and high COP in the optimal configuration, representing a good compromise as a mid-term R404A replacement. Górny et al. [10] confirmed the suitability of a method for assessing the lubricity of POE with R404A and R452A, which is essential in the selection of oil for new refrigerants and long-life refrigeration systems with low energy consumption. Recently, Maiorino et al. [11] presented a comprehensive review about the state of the art of the technologies used in the refrigerated transport sector, identifying the main issues and possible solutions to improve the sustainability of the cold chain.

Nasuta et al. [12] developed an Excel-based Life Cycle Climate Performance calculation tool for transport refrigeration and bus air conditioning applications. They proved that indirect emissions (for electricity generation) dominate total emissions. Tassou et al. [13] identified several ways to reduce energy consumption in refrigerated transport, such as utilizing the exhaust heat, utilizing phase change materials, or hybridizing system arrangements, and recommended further investigation into solar energy-driven systems. Wu et al. [14] determined that CO_2,e emissions caused by the energy consumption to power the compressor and carry the refrigeration unit resulted in a large part of the total. Moreover, refrigerators driven by auxiliary engines have higher CO_2,e emissions than those operated by the vehicle engine or electricity.

Cenex [15] included electrification as one of the cleaner options for the future, replacing the auxiliary diesel engine with electricity from a battery, fuel cell, or even a solar photovoltaic (PV) array to run the refrigeration compressor. Njoroge et al. [16] state that renewable energies powering refrigeration systems must be installed to transport perishable goods. The solar PV array is mounted on the top of the vehicle, whereby an inverter system is used to convert the DC output to AC. Excess energy is stored in the batteries to supplement any shortfall. A few patents have been registered with PV technology. Blasko et al. [17] included a power-management controller to select from two electrical power sources to power two motors (compressor and fan).

Solar refrigeration technology comprises a compound system in which solar power produces cooling [18]. Solar PV cooling (also known as solar-assisted vapor compression refrigeration) shall consist of four essential components: PV modules, a battery, an inverter circuit, and a vapor compression system. Lazzarin [19] identified comparable costs between the PV-driven system concerning the solar thermal system. Although the specific cost of PV is much higher than solar thermal, it is lowering, and its efficiency is improving continuously. Infante Ferreira and Kim [20] agreed that vapor compression cycles combined with PV collectors lead to the economically most-attractive solutions. According to Kim and Infante Ferreira [21], the most significant advantages of PV panels combined with conventional vapor compression systems are simplicity and relatively high overall efficiency. However, drawbacks like the necessity of batteries (thermal or electrical) and the price of PV panels prevent the extension of these systems.

Salilih and Birhane [22] proved that solar radiation intensity increases the compressor rotational speed when directly connected to PV panels. Its energy performance, cooling capacity, and power consumption are also variable; therefore, a battery can decouple refrigeration parameters from solar intensity. Su et al. [23] confirmed this assumption experimentally and emphasized the influence of ambient temperature on the cooling capacity and energy performance.

PV-driven refrigeration has not been extensively studied in refrigerated transport, but it presents promising results in other refrigeration, air conditioning, and heat pump applications. Mahmoudi et al. [24] studied a 170 m^2 PV integration for a cold storage

facility, and the energy consumption decreased by around half, with a 5.2 years payback period. Novaes Pires Leite et al. [25] found robust techno-economic viability in integrating air-conditioning and solar PV systems, especially in tropical latitude regions. Essential variables are energy price, annual adjustment, PV cost, and solar panel efficiency.

PV refrigeration has been compared with other cooling technologies, showing benefits in different aspects. Regarding costs of investment, Lazzarin and Noro [26] found PV-driven technologies because they offer similar cooling production at the expense of about half that of the best thermally driven system. The unexpected drop in PV module costs completely changed the competition between thermally or electrically driven solar cooling systems. Reda et al. [27] proved that the PV-driven heat pump is more economically viable than solar absorption for office building applications in the Northern climate. Riva et al. [28] concluded that PV-driven systems present almost half the CO_2,e emissions compared to solar absorption heat pumps, and economies of scale offer opportunities to improve them.

Refrigerated transport must reduce greenhouse gas emissions to meet global sustainability targets. However, they are still strongly dependent on fuel consumption. A few past works have proved how refrigeration systems can be efficiently powered by solar energy, but this is not studied in detail in refrigerated transport, where other parameters, such as weight, become vital for the resulting CO_2,e emissions. From energy and economic perspectives, this work aims to model and analyze an innovative hybrid refrigerated van equipped with a PV system that powers the refrigeration unit. Moreover, the renewable source is sized considering different PV technologies. The charge and discharge curves are evaluated as a function of the required cooling load, battery capacity, impact of temperature on performance, and comparison between lithium and lead-acid batteries.

2. Comprehensive Energy Model

A comprehensive energy model was developed to optimize the design of a photovoltaic system coupled to the refrigeration unit of a commercial van to reduce energy consumption and CO_2,e emissions (Figure 1). A photovoltaic system to provide a gross peak power of 600 W was considered for this investigation. The main characteristics of the van and the photovoltaic system can be found in Appendix A.
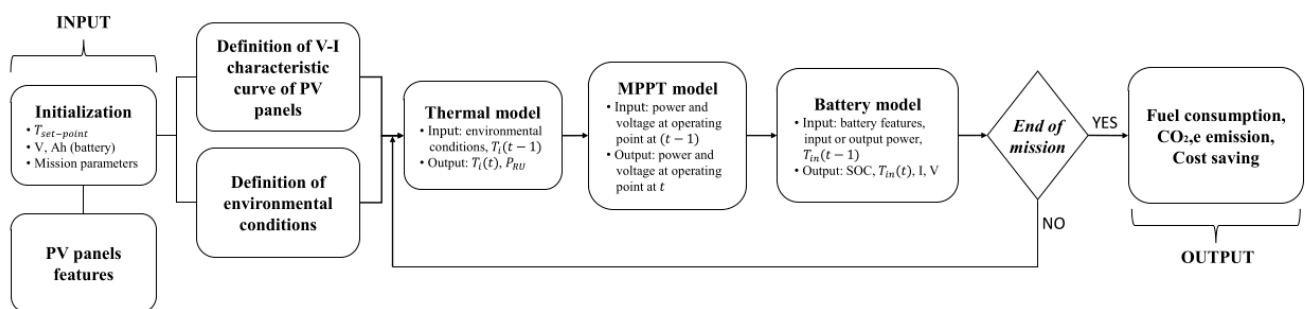

Figure 1. Model flow diagram.

The energy model is composed of several sub-models. The first is the thermal model (detailed equations can be found in Appendix B). It has the objective of evaluating the transient behavior of the internal temperature of the cold room using the boundary conditions and the required cooling power. The thermal model is based on a heat balance equation with lumped parameters, Equation (1).

$$m_{in} c_{in} \frac{\partial T_{in}}{\partial t} = \dot{Q}_{aux} + \dot{Q}_{defrost} + \dot{Q}_{door} - \dot{Q}_{RU} + \dot{Q}_{in-w} + \dot{Q}_{in-c'} \tag{1}$$

where m_{in}, c_{in} and T_{in} are the mass, the specific heat capacity, and the air temperature inside the cold van, respectively. $\dot{Q}_{aux}$, $\dot{Q}_{defrost}$, and $\dot{Q}_{door}$ are the thermal loads due to the auxiliary components, the defrost cycle, and the door opening, respectively, $\dot{Q}_{RU}$ is the cooling power, and $\dot{Q}_{in-w}$ and $\dot{Q}_{in-c}$ are the thermal loads due to the heat exchange

with the walls and the cabinet, respectively. The initial conditions are calculated for any external condition (airspeed, irradiance, temperature), considering the case in which the temperature profile in the walls follows a hysteretic cycle. This cycle oscillates around the set-point air temperature following the refrigeration ON/OFF cycle. Figure 2 represents the thermal fluxes to which the cold chamber is subjected.
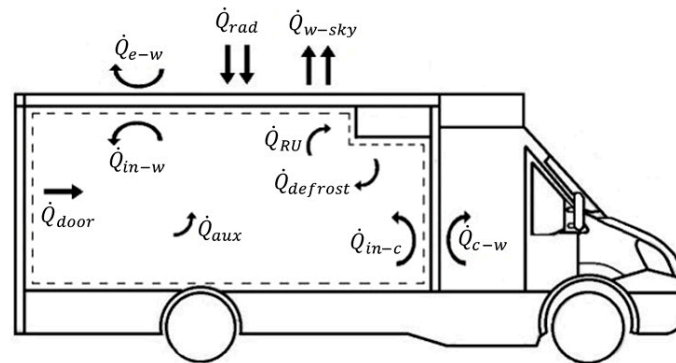

Figure 2. Heat flow schematic.

The first validation of this sub-model was carried out with an experimental test in static mode performed in March 2020. The electric power absorbed by the refrigeration unit and air temperature at the inlet and outlet of the evaporator was measured. The inputs were the external conditions, temperature and speed of the internal/external air, irradiance (obtained by the PVGIS-SARAH database), set-point temperature, and initial operating conditions. The vehicle can set three cooling levels according to the targeted internal and external conditions. These are maximum cooling power during the pull-down stage, an intermediate operation when the system is switched on during hysteresis cycles, and a minimum level regulating the power supply frequency.

According to an MPPT (Maximum Power Point Tracking)-based logic, the model identifies the amount of power provided by the PV system, the power supplied or absorbed by the battery, and the power provided by the van's internal combustion engine.

A battery model (Appendix C) provides the State of Charge (SOC) and the voltage (V) of the battery. In the charging and discharging phase, two different behaviors were considered for lithium and lead-acid batteries.

The accumulation of the results provided by the model during an extended period allows to calculate the associated fuel consumption and CO_2,e emission, together with the value of the electricity losses at the PV panels, battery (electrical connections), refrigeration unit, inverter, and relative savings in electricity over the entire month, excluding the battery charge. Fuel consumptions due to van traction and power refrigeration system depend on the specific route. The input data are the time of arrival at each checkpoint (points at which the parameters are evaluated and then kept constant until the next checkpoint), average speed of the van, distance between two successive checkpoints, and load carried.

The CMEM (Comprehensive Modal Emission Model) approach [29], used to estimate the fuel consumption and emissions related to the vehicle's operation, is based on several parameters that vary according to the specific vehicle, engine, and operation considered. Most of these parameters are related to the vehicle and the engine characteristics (engine size, vehicle mass and frontal area, aerodynamic drag coefficient) and are easily obtainable. Other parameters refer to vehicle operation, for example, and can be deduced through ECU readings. Such a method is called "comprehensive" as it can be applied to all the vehicles. Based on this approach, the instantaneous rate of fuel consumption FR when traveling at a constant speed v with a specific load l is estimated using Equation (2).

$$FR = \frac{\xi}{LHV_{fuel}\rho_{fuel}}\left(kN_{en}D_{en} + \frac{0.5C_d\rho Av^3 + (\mu + l)v(g\sin\Phi) + gC_r\cos\Phi}{1000\eta_{mec}\eta_g}\right), \quad (2)$$

where ξ is the mixture ratio, LHV_{fuel} lower heating value of the fuel, ρ_{fuel} density of the fuel, k engine friction factor, N_{en} engine rotation speed, D_{en} engine displacement, C_d coefficient of aerodynamic drag, ρ air density, A area of the front surface of the van, v speed of the van, μ system weight (panels + battery + inverter), l transport load, g acceleration due to gravity, Φ street angle, C_r Rolling resistance coefficient, η_{mec} vehicle transmission efficiency, and η_g overall efficiency of the internal combustion engine.

The fuel consumption F, for a distance (d) and certain speed (v), is then calculated as Equation (3) shows [30].

$$F = FR\frac{d}{v}. \tag{3}$$

The total fuel consumption of the trip is given by the sum of the consumptions in the single i-th sections, Equation (4).

$$F_{tot} = \sum_i F_i. \tag{4}$$

Considering a conversion factor equal to 1.5 dm^3 kg^{-1}, a unit cost of methane Cu of 0.99 € per kg referred to the last quarter of 2018 in Italy [31], and an emission factor f of 56.1·10^{-3} kgCO$_2$,e MJ^{-1} [32], the cost and carbon footprint of the trip can be obtained from Equations (5)–(7).

$$m_{fuel,drive} = F_{tot}/1.5, \tag{5}$$

$$C_{drive} = m_{fuel,\,drive}Cu, \tag{6}$$

$$m_{CO_2,drive} = f\,LHV_{fuel}m_{fuel,drive} \tag{7}$$

On the other hand, the fuel consumption due to the operation of the refrigeration unit is given by Equation (8).

$$m_{fuel,RU} = \frac{P_{RU}}{LHV_{fuel}\eta_{real}}, \tag{8}$$

where P_{RU} is the electric power absorbed by the refrigeration unit without considering the PV generation, and η_{real} efficiency of the internal combustion engine, fixed at 20%, can be changed and made variable according to the operating conditions.

The model was validated by a test carried out in early March 2020, during which the total fuel consumption was recorded. It involved a single delivery transport of 150 kg of frozen pastry products at a temperature of −20 °C. The comparison of the results obtained with the model and measurements is shown in Table 1.

Table 1. Comparison between measured data and results obtained from the model.

Parameter	Model	Test
Total distance (km)	90.2	
Total time (min)	63	
Departure	11.10	
Drive (kg)	10.02	Not applicable
Refrigeration (kg)	0.46	Not applicable
Total consumption (kg)	10.5	10.1
Total cost (€)	9.96	10.0
Total CO$_2$ emissions (kg)	28.1	28.2

The model obtains a 4% increase in consumption compared to the test (evaluated by OBD scanner). This error can be considered acceptable in an initial modeling and simulation phase.

3. Results and Discussion

The potential of the innovative refrigerated van requires validation using real routes.

Two situations were proposed. The first is a single delivery scenario characterized by a single trip from the production or distribution center to the point of sale. The second is a multiple deliveries scenario in which three points of sale were considered, assuming that the refrigerated products unloading operations last 10 min. Both also consider returning to

the origin with the refrigeration unit off (all product is delivered). At the origin, the battery that powers the refrigeration unit is connected to an external electrical outlet to be fully charged for the following day. Moreover, the van performs one trip a day on weekdays.

The operating conditions depend on the path considered for the simulation and extracted from Google Maps and the PVGIS-SARAH database. The first provides the traveled distance and the vehicle's speed. At the same time, the second is used to know the solar radiation, ambient temperature, and wind speed, averaged over the previous three years.

Meneghetti and Ceschi [33] recommended selecting the route with the minimum fuel consumption for traction and refrigeration. Energy savings are affected by the location of the sale points, departure time, number of deliveries per trip, seasonality, and location of the delivery network. The locations considered in the trips are shown in Table 2. For this investigation, the road O-D1 (72.1 km road distance) was chosen as the single-delivery scenario and O-D2-D3-D1-O (97.5 km road distance) for the multiple-deliveries scenario.

Table 2. List of locations considered for the trips. All locations are in Campania, Italy.

Code	Address	Coordinates
O	Via Santa Maria La Neve, Tramonti (SA)	40.70, 14.66
D1	Via Benedetto Croce 63, Avellino (AV)	40.92, 14.78
D2	Corso Giuseppe Garibaldi 12, Castellammare di Stabia (NA)	40.70, 14.48
D3	Via Salvatore D'Alessandro 42, Nocera Inferiore (SA)	40.75, 14.63

3.1. Single-Delivery Scenario

This section analyses the results of the comprehensive energy model applied to the single-delivery scenario to find the optimal photovoltaic system design.

3.1.1. Selection of PV Panels

In the first step, three different models of PV panels are considered (their main characteristics can be found in Table A3-Appendix A), assuming the system employs a 100 Ah 24 V lead-acid battery. Type A requires 327.3 kWh of energy from the power grid in a year to charge the battery before each departure. Model B requires 341.4 kWh, and model C requires 324.4 kWh, implying that model B has lower electricity production for a single trip.

Figure 3 shows the energy produced by the three considered modules per month. The choice of the PV panel does not significantly influence the total van weight; consequently, the fuel consumption is not affected. The number of panels positioned on the roof, bound to the available surface, is calculated according to the energy generated.

The common costs for the PV system accessories are shown in Table 3, and the cost associated with each PV panel type is shown in Table 4. There is a significant difference in the cost among the different models. In detail, the more expensive PV panel is also that one which shows the higher energy production. Therefore, this analysis influences the payback period of the proposed solution. Moreover, it should be highlighted that the expected cost of any PV panel represents between 25% and 43% of the final cost.

Table 3. Common costs for PV system accessories.

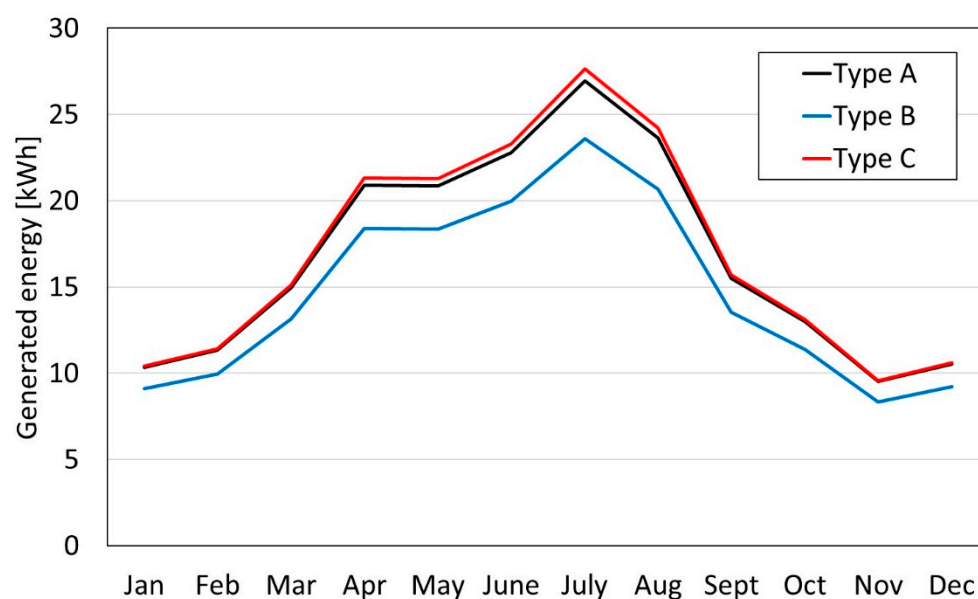| Component	Unit Cost [€]	Units	Total Cost [€]
MC4 connectors	4.80	1	4.80
Extension cable	1.20	14	16.80
Double-sided adhesive	18.00	5	90.00
Inverter-MPPT	473.72	1	473.72
24 V 100 Ah battery	480.00	1	480.00
Total			1065.32

Figure 3. Energy generated by different PV modules.

Table 4. Investment required for each PV panel model.

PV Panel	Unit Cost [€]	Units	Cost PV Panels [€]	Total Cost [€]
Type A	430.00	5	2150.00 €	3215.32
Type B	290.00	5	1450.00 €	2515.32
Type C	260.00	12	3120.00 €	4185.32

Attending to the costs and the electricity produced, a simulation is performed to evaluate the payback period of the different PV panels, shown in Table 5, assuming a cost of the electricity from the power grid of 0.061 € per kWh. The PV panels reduce the annual costs of the van by about 7%. Still, the initial economic benefits are not considerable, so the payback period is not at an acceptable level, longer than the usual lifetime of a van. If necessary, the only model acceptable from an economic perspective in a refrigerated van doing single deliveries (one per day) would be model B, which could be compensated before replacing the refrigerated van. For this reason, model B was chosen as the best option for PV panel type; therefore, all the results presented after this were obtained considering only this model.

Table 5. Economic analysis.

Parameter	Baseline	Type A	Type B	Type C
Investment cost [€]	NA	3215.32	2515.32	4185.32
Power grid cost [€]	NA	19.97	20.82	19.79
Annual costs [€]	1606.46	1488.46	1492.68	1488.06
Net Present Value [€]	NA	118.00	113.78	118.40
Payback period [years]	NA	27	22	36

With the selected components, it is possible to evaluate to what extent the PV system can meet the electricity needs. Figure 4 shows that the PV panels produce around half the energy the batteries require for most of the months. The worst results are for the months of winter. Moreover, the energy losses represent just a tiny percentage of the electricity produced.
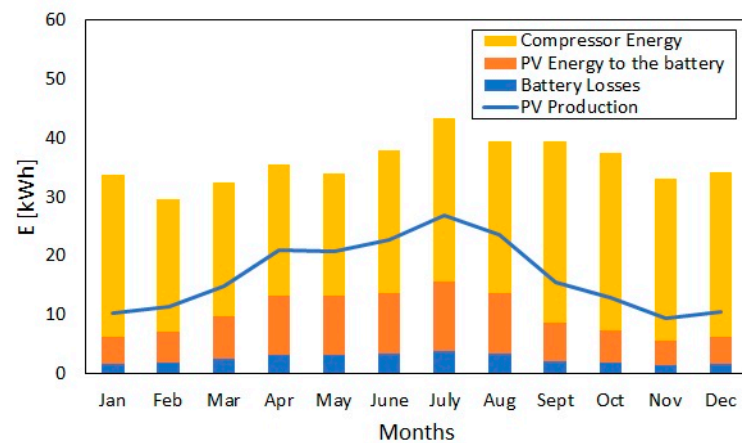
Figure 4. Monthly distribution of energy in the system: energy required to move the compressor of the refrigeration unit, energy produced by the PV panels and sent to the battery, battery losses, and total energy produced by the PV panels.

The electric power required by the refrigeration unit and the power generated by the PV panels are shown for the previous route considering a specific day as an example (see Figure 5). As it can be seen, the compressor follows hysteretic cycles to keep the refrigerated compartment temperature at acceptable levels (Figure 5a). Then, the power provided by the PV panels decreases from 0.37 to 0.30 kW because they are heated during the trip, and their efficiency is reduced (Figure 5b).
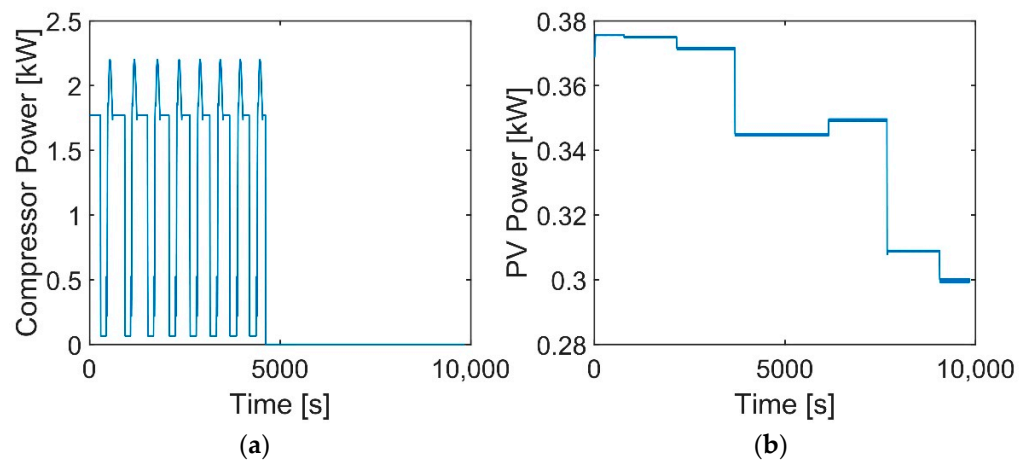

Figure 5. Power required by the refrigeration unit (**a**) and solar power available (**b**).

3.1.2. Selection of Batteries

After comparing PV panel models, two types of batteries are analyzed, i.e., lead-acid and lithium. Figure 6 presents current, voltage, state of charge (SOC), power, and temperature variations for the proposed single-delivery scenario. The lead-acid battery has more significant variations in terms of voltage, while the lithium battery is the one that presents a similar phenomenon according to the current. The SOC values of a lead-acid battery are always lower than lithium, while the power of both remains at comparable values. Finally, the lead-acid battery temperature is about 4 °C higher than lithium.

Considering an economic analysis performed for the three types of PV panels, the payback period of each battery is analyzed, considering 670 € per kWh nominal for the lithium type and 200 € per kWh nominal for the lead-acid. Figure 7 shows the payback period as a function of the capacity. It can be noticed that using a 100 Ah lead-acid battery allows for achieving the minimum payback period, which is 26 years. In contrast, for a lithium battery, the payback period is constantly increased, at a minimum of 28 years for 50 Ah capacity.
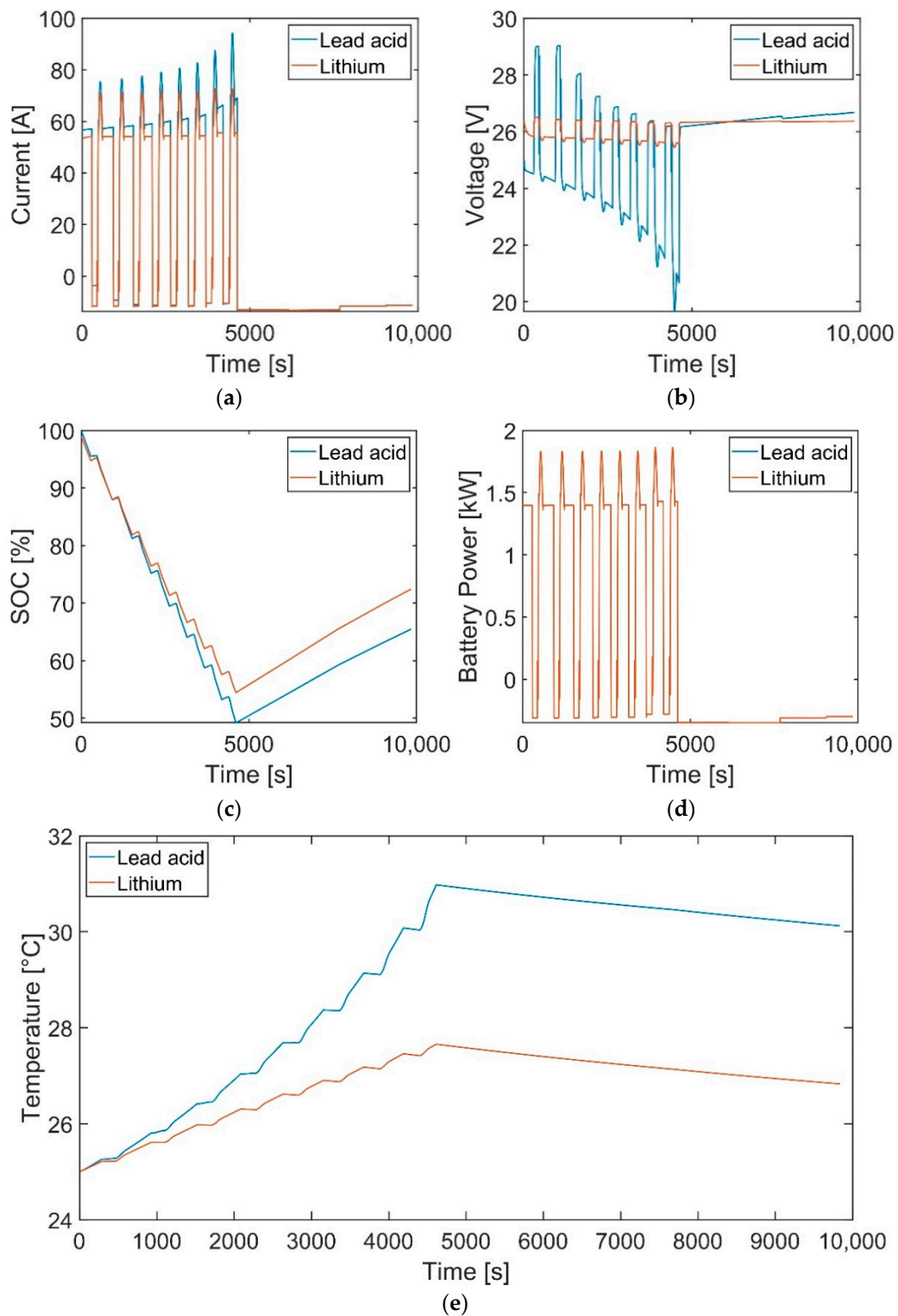
Figure 6. Comparison of electrical and thermal behavior between lead-acid and lithium batteries: (**a**) Current, (**b**) voltage, (**c**) SOC, (**d**) power, and (**e**) temperature.
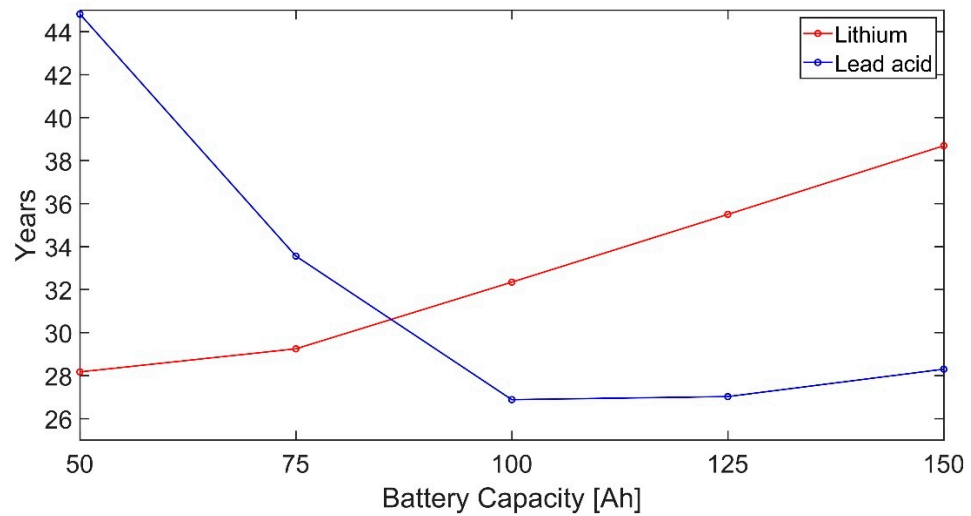
Figure 7. Behavior of the payback period of the lithium and lead-acid batteries according to different capacities.

The Round Trip Efficiency (*RTE*) parameter is proposed for evaluating the suitability of the different batteries. Two parameters can be considered: one that only considers the amount of input and output energy at the battery (RTE_b), and another the available solar energy (RTE_{tot}). Both factors are added to the energy absorbed from the grid, as shown in Equations (9) and (10).

$$RTE_b = \frac{E_b}{E_{Reintegrated} + E_{PV-b}},\qquad(9)$$

$$RTE_{tot} = \frac{E_b}{E_{Reintegrated} + E_{sol-b}},\qquad(10)$$

where E_b is the energy provided by the battery to the refrigeration unit; $E_{Reintegrated}$ is the energy provided by the power grid to recharge the battery before the departure; E_{PV-b} is the energy provided by the photovoltaic system to charge the battery; and E_{sol-b} is the available solar energy to recharge the battery. The difference between E_{PS-b} and E_{sol-b} is that E_{PV-b} is affected by the internal losses due to the efficiencies of the components.

The results are reported in Figure 8 for lead-acid and lithium batteries for each month and different capacities.
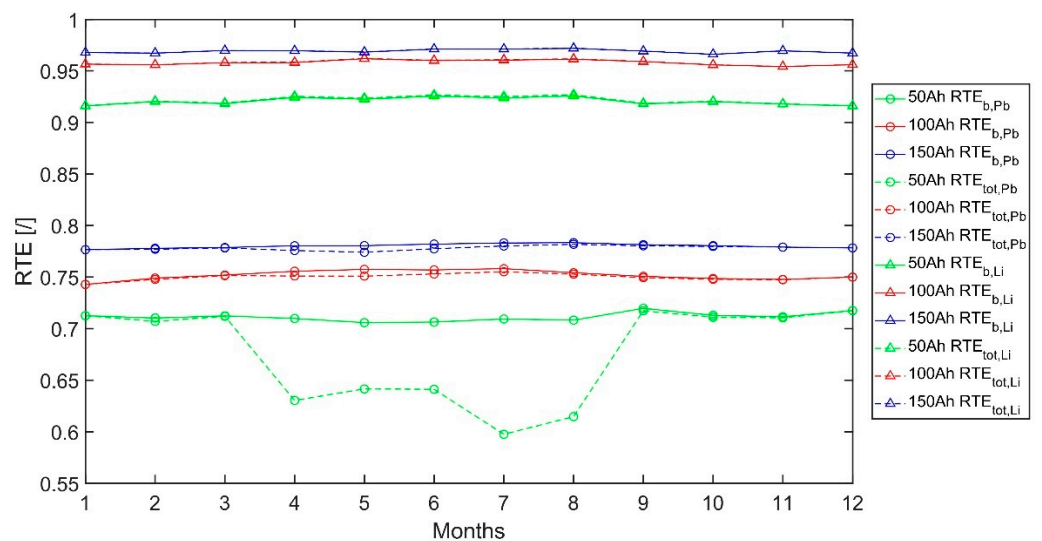

Figure 8. Comparison of RTE values among several battery solutions for both lead-acid and lithium types.

From Figure 8, it is evident that the lithium battery performs better than the lead-acid one. Indeed, the former shows efficiencies between 91.5% and 97%, whereas the latter shows efficiencies between 70% and 77%. Moreover, as expected, the efficiency increases as the capacity of the battery increase for both types. RTE_b does not vary much between months since the energy the battery provides is almost constant throughout the year. The deviations between RTE_b and RTE_{tot} are shown only during summer, since there is an increase in the available solar energy. In detail, a significant difference can be observed for the smallest lead-acid battery (50 Ah). The latter switches into charge mode very often. Therefore, it is characterized by a high state of charge, and it switches into charge mode with a constant voltage if the available solar energy is high. In this state, the current is reduced to protect the battery from an overvoltage, so RTE_{tot} decreases. In the end, a 100 Ah lead-acid battery provides the best techno-economical compromise.

3.1.3. Overall Results

Table 6 summarizes all information obtained per month for the final solution considered, i.e., model B as PV panel type and a 100 Ah 24 V lead-acid battery. This choice mainly comes from the economic analysis for the PV panels, whereas for the battery, some other factors were also considered (RTE). Savings refer to the economic savings evaluated by adopting the proposed solution concerning the original configuration of the van, considering that the grid is fully charged every day before the departure. E_{RU} represents the energy absorbed by the refrigeration unit; E_{PS} is the energy provided by the photovoltaic system to run the refrigeration unit or recharge the battery; and E_b is the energy supplied by the battery to run the refrigeration unit. Losses are attributed to each section of the photovoltaic power supply system.

Table 6. Monthly electric consumption in the scenario considered.

Parameter	Jan	Feb	Mar	Apr	May	Jun	Jul	Aug	Sep	Oct	Nov	Dec
Distance [km]						72.10						
Time [min]						77.00						
E_{RU} [kWh]	33.7	29.1	32.4	35.5	34.0	38.0	43.3	39.6	39.1	37.7	33.0	33.8
E_{PS} [kWh]	5.2	5.3	7.4	10.4	10.4	11.6	13.4	11.6	9.0	7.4	5.2	5.8
E_{bat} [kWh]	0.9	0.8	0.8	0.7	0.6	0.7	0.7	0.7	0.8	0.9	1.0	1.0
$E_{Reintegrated}$ [kWh]	30.4	24.0	26.4	23.9	21.9	24.7	24.8	24.9	26.6	30.6	29.1	31.8
$Losses_{PV}$ [kWh]	0.6	0.6	0.8	1.1	1.1	1.2	1.5	1.3	1.0	0.8	0.6	0.6
$Losses_{bat}$ [kWh]	0.1	0.1	0.1	0.1	0.1	0.1	0.1	0.1	0.1	0.1	0.1	0.1
$Losses_{RU}$ [kWh]	9.7	8.4	9.3	10.1	9.7	10.7	12.2	11.2	11.2	10.7	9.5	9.7
Losses inverter [kWh]	3.2	2.8	3.2	3.6	3.4	3.8	4.2	3.9	3.6	3.6	3.1	3.4
Losses tot [kWh]	13.6	11.8	13.4	14.9	14.3	15.9	18.0	16.4	15.7	15.5	13.2	13.8
Savings [%]	4.0%	12.1%	18.4%	32.8%	35.6%	34.9%	39.2%	30.4%	22.7%	12.9%	5.2%	5.7%

Figure 9 shows the results that summarize the monthly electricity absorbed by the refrigeration unit, produced by the PV system, and reintegrated from the grid. The latter represents the energy the battery provides, which is fully charged by the grid before each departure, to run the refrigeration system when the energy provided by the PV panels is insufficient. The fuel consumption for refrigeration in the summer months is slightly increased compared to the winter months. Refrigeration consumption is almost entirely cut thanks to the energy supplied by the battery connected to the PV panels, even if refrigerator energy consumption represents only 10% of total consumption.

Figure 10 depicts the economic and environmental feasibility of the proposed solution. Considering the single-delivery scenario presented, there is a total cost saving of about 100 € per year. Undoubtedly, the savings would be of no minor importance for longer trips and carrying out more than one daily trip. Furthermore, the economic saving is strongly affected by the unit cost of methane, which should increase as the unit cost increases. Therefore, higher cost savings should be expected with an increasing unit cost of methane.
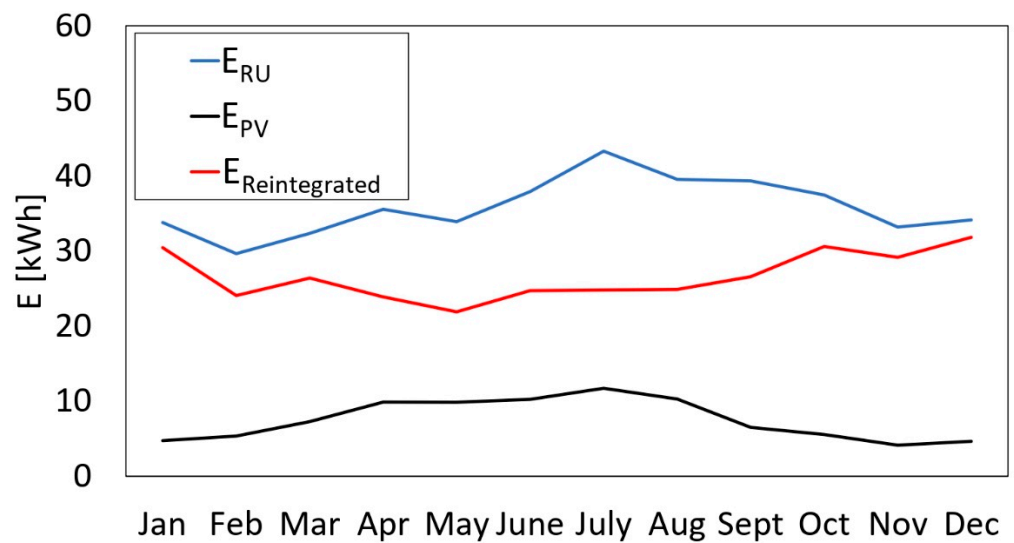
Figure 9. Monthly electricity absorbed by the refrigeration unit, produced by the PV system, and reintegration from the grid.
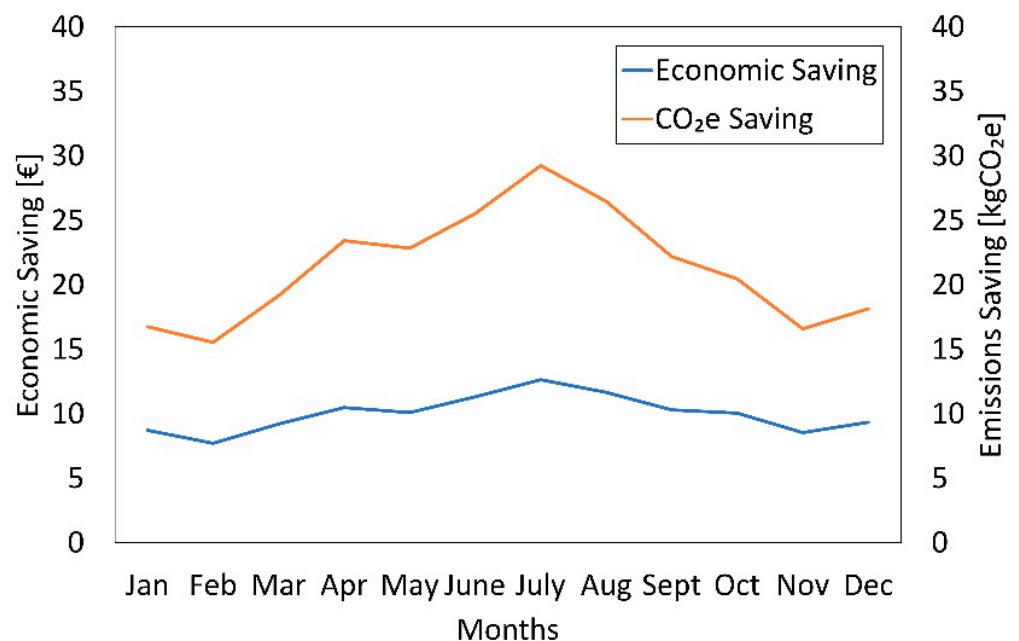

Figure 10. Monthly economic and CO_2 emissions savings provided considering single-delivery trips. The refrigerated van represents the reference solution without the PV panels installed.

From the environmental perspective, it is possible to reduce CO_2,e emissions by about 150 to 250 kg per year; even in this case, the situation could improve considering longer trips and carrying out more than one trip per day.

3.2. Multiple-Deliveries Scenario

In this case, a route with multiple deliveries is considered, selecting the order of deliveries according to the most optimal route for minimizing the total distance and time traveled (which is not discussed since it is outside the aim of this work). Identifying the optimal design for PV panel and battery types is not performed, since the single-delivery scenario was used to select the best solution. The same configuration was adopted to evaluate the performances in a multiple-deliveries scenario.

Figure 11 shows that the electricity required by the cooling unit has a minimum variation throughout the year. A peak is observed in July, but the cooling demand is only

approximately 30% higher than in February (Figure 11a). The electricity taken from the grid represents between 50% and 63% of the total required. The electricity generated by the PV panels varies between 16% and 32% of the necessary cooling.
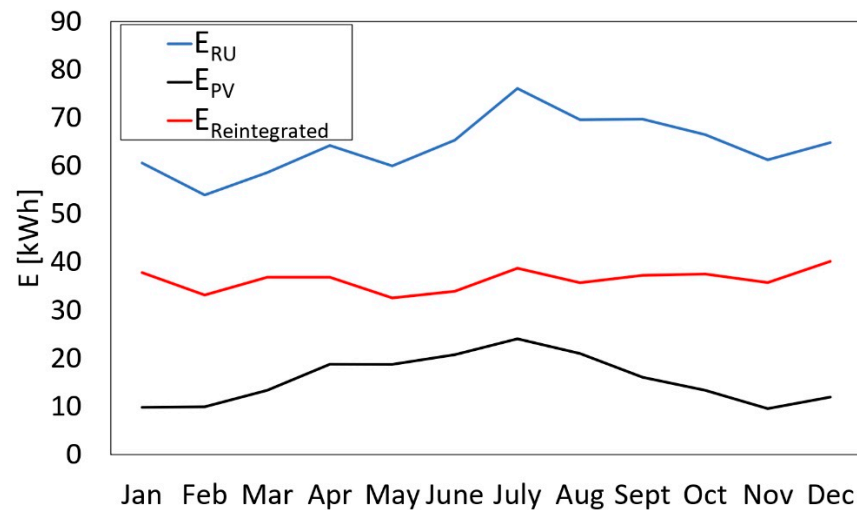
(a)
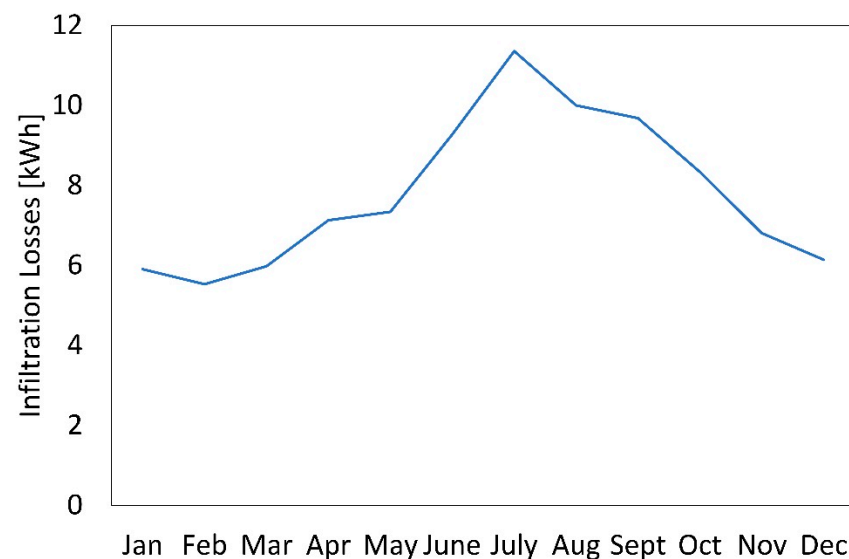
(b)

Figure 11. Monthly electricity absorbed by the refrigeration unit, produced by the PV system and reintegration from the grid (**a**) and monthly infiltration losses during the unloading operations of the products in each delivery (**b**).

Moreover, there is a significant difference for the single-delivery scenario, represented by the heat gain due to the unloading operations of products considered in a multiple-deliveries scenario. The cooling required due to the air infiltration (opening the doors for charge/discharge load) represents between 23.5% and 33.6% of the total (Figure 11b).

Figure 12 shows the economic and CO_2,e savings compared with the same van without PV panels. As seen, there is a yearly economic saving of about 138 €. Undoubtedly the savings would be of no minor importance for longer trips and carrying out more than one delivery per day. Moreover, like in the single delivery scenario, higher cost savings should be expected with an increasing unit cost of methane.

Figure 12. Monthly economic and CO_2,e emissions savings provided considering the multiple-deliveries scenario. The refrigerated van represents the reference solution without the PV panels installed.
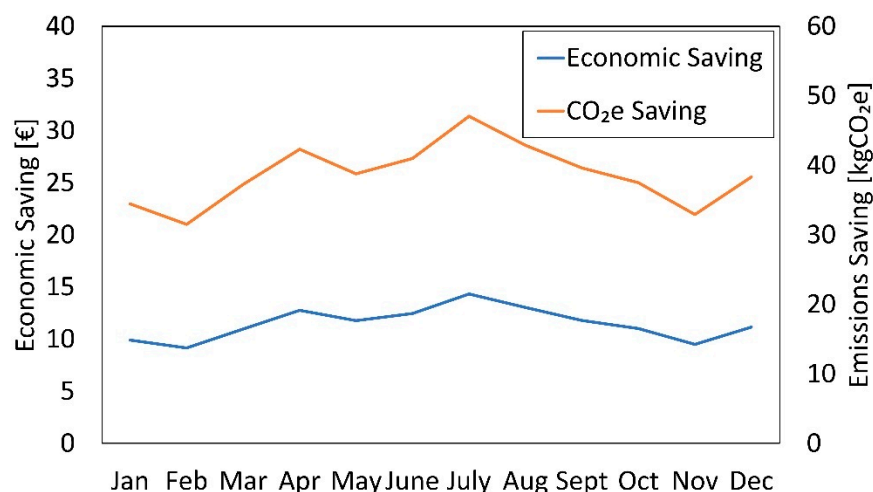
In addition to the financial information, from the environmental point of view, saving about 463.6 $kgCO_2$,e per year is possible, which is more noticeable during the peak in the spring and summer months. Since the economic and environmental savings are caused by the increase of energy produced by the PV panels, similar trends are observed. Moreover, the results could improve considering longer trips and carrying out more than one multiple-delivery per day.

4. Conclusions

The food refrigerated-transport sector and the entire food supply chain demand a sustainable transition to decrease the dramatic figures in total greenhouse gas emissions. Current solutions aim for the electrification of vehicles, including onboard batteries. This paper presents a comprehensive energy model (thermal-electrical) that simulates a hybrid refrigerated van and calculates fuel energy consumption, costs, and CO_2,e emissions for any type of use. The model can be seen as an initial supporting tool aiming to design a sustainable refrigerated-transport system for food and perishable goods. The model uses the set-point temperature, battery and photovoltaic panel characteristics, and trip as input parameters. Then, the V-I characteristic curve of the photovoltaic panels and the environmental conditions are determined. The thermal model of the refrigerated cabin, and the electrical model, including batteries and photovoltaic panels, are coupled.

This paper contrasted different photovoltaic panels and electric battery technologies. A significant difference in the payback period of the photovoltaic panels was observed. For the economic analysis, all technologies produce comparable electricity annually, and the factor determining the most suitable panel is the investment cost. Then, regarding batteries, lead-acid battery was highlighted over lithium as the most convenient technology, optimizing the capacity. To test the effectiveness of the model, two different scenarios were investigated: a single-delivery scenario and multiple-delivery scenarios.

Considering thermal and electricity losses, the total net savings for a single-delivery scenario is around 100 € per year, and 150 to 250 $kgCO_2$,e emissions are avoided. In a more realistic scenario that simulates multiple deliveries, the yearly economic saving is increased to 138 € and 464 $kgCO_2$,e reduction of carbon footprint. It is proved that the batteries and the photovoltaic production are insufficient to provide the cooling required by the refrigeration unit. However, along with higher cooling requirements, electricity production is maximized in the summer.

Developing a comprehensive energy model represents a fundamental step toward the optimal design of a hybrid refrigerated van. It simulates different technologies for photovoltaic production and energy storage systems to identify those most suitable for different applications in delivery scenarios. The hybridization of refrigerated vans can

decrease carbon emissions along the cold chain. Still, their optimal design is crucial, since the investment costs can hinder the transition to these eco-friendly systems. Therefore, every component must be fully optimized from an economic and energy perspective. The proposed comprehensive energy model provides a helpful tool for simulating different solutions for different applications and identifying the optimal one for a specific need. In this work, just some examples of model implementation show the potential of the comprehensive approach. Future works should be addressed to test many other alternative scenarios with different operating conditions and adopted technologies, intending to depict a widespread representation of the savings achievable by hybridizing refrigerated vans. Moreover, considering the entire food supply chain, the environmental performance of such a solution should also be evaluated. In this case, the proposed model can be seen as an initial supporting tool to be integrated into a broader context to reduce the environmental impact of the food transport phase and get closer to developing a sustainable food supply chain.

Author Contributions: A.M. conceived the idea and helped with the development of the methodology and the discussion of the results. A.M.-B. wrote the draft of the paper and helped with the discussion of the results. F.P. developed the thermal model, helped to develop the comprehensive model, ran some simulations, and analyzed the results. M.G.D.D. helped with the finalization of the manuscript and the discussion of the results. A.A. helped develop the comprehensive model, running some simulations and analyzing the results. C.A. supervised the entire work. All authors have read and agreed to the published version of the manuscript.

Institutional Review Board Statement: Not applicable.

Informed Consent Statement: Not applicable.

Conflicts of Interest: The authors declare no conflict of interest.

Nomenclature

Symbols

A	amplitude of the exponential area [V]
B	constant of time in the exponential area [Ah^{-1}]
c	specific heat [$J\ kg^{-1}\ K^{-1}$]
Cd	coefficient of aerodynamic drag [-]
C_{inf}	infiltration coefficient [$m^{1/2}\ s^{-1}$]
C	cost [€]
$Corr_R$	resistance correction parameter [Ah^{-1}]
$Corr_K$	polarization constant correction parameter [A^{-1}]
Cr	rolling resistance coefficient [-]
Cu	unit cost of methane [€ kg^{-1}]
d	distance [m]
D_{en}	engine displacement [m^{-3}]
E	electric energy [kWh]
Exp	exponential voltage [V]
f	emission factor [$kgCO_2$,e MJ^{-1}]
F	fuel consumption [kg]
FR	instantaneous rate of fuel consumption [$kg\ s^{-1}$]
g	gravity [$m\ s^{-2}$]
G	solar radiation [$W\ m^{-2}$]
h	convective heat transfer coefficient- [$W\ m^{-2}\ K^{-1}$]
H	door's height [m]
i	current [A]
*i**	filtered current [A]

it	actual charge of the battery [Ah]
j	specific enthalpy [kJ kg^{-1}]
k	engine friction value [-]
K	polarization constant [V Ah^{-1}]
l	transport load [kg]
LHV	lower heating value [kJ kg^{-1} or MJ kh^{-1}]
m	mass [kg]
$\dot{m}$	mass flow rate [kg s^{-1}]
N$_{en}$	engine rotation speed [rps]
P	electric power [W]
Q	battery capacity [Ah]
$\dot{Q}$	heat transfer [W]
$\dot{q}$	heat flow rate [W m^{-2}]
R	internal resistance of the battery [Ω]
RTE	Round Trip Efficiency [-]
s	width [m]
S	surface [m^2]
SOC	State Of Charge [%]
T	temperature [°C or K]
t	time [s]
v	speed [m s^{-1}]
V	voltage [V]
$\overline{V}$	constant voltage [V]

Greek symbols

η	efficiency [-]
η_i	Coulombic efficiency [-]
σ	Stephan–Boltzmann constant [W m^{-2} K^{-4}]
ρ	density [kg m^{-3}]
τ	characteristic time constant of the considered battery [s]

Subscripts

AG	air gap
amb	ambient
aux	auxiliary components
b	battery
B	body
back	back side
c	cabinet
conv	conversion
defrost	defrost system
door	door
drive	drive
e	external
en	engine
front	front side
fuel	fuel
g	global
in	inside
Li	Lithium battery
mec	mechanical
mp	maximum power
nom	nominal
oc	open circuit
Pb	lead-acid battery
PV	photovoltaic
rad	radiation
real	real or indicated
ref	reference

Reintegrated	reintegrated from the grid
roof	roof
RU	refrigeration unit
sc	short circuit
sol	solar
sky	sky
w	wall
Abbreviations	
CO_2,e	Carbon dioxide equivalent
MPPT	Maximum Power Point Tracking
PV	Photovoltaic

Appendix A. Refrigerated Van and PV System Features

The characteristics of the refrigerated van are shown in Table A1.

Table A1. Main characteristics of the refrigerated van.

Parameter	Characteristics
Engine (F1CFA401A)	Four-stroke bi-fuel spark ignition (petrol-methane) maximum power (methane): 100 kW (136 CV) @ 2730–3500 rpm maximum torque (methane): 350 N·m @ 1500–2730 rpm Displacement: 2998 cm^3
Refrigerated cabin	Reinforced isothermal class F (thermal transmittance of the walls between 0.29 and 0.4 W m^{-2}K^{-1}), minimum temperature inside the cabin of -20 °C
Refrigeration unit	R-452A refrigerant, hermetic compressor with inverter (30 to 80 Hz)
Refrigeration unit power supply	Electric mains or dedicated auxiliary alternator, directly driven by the heat engine

Then, the internal composition of the refrigerated cabin walls considered in the model is shown in Table A2.

Table A2. Characteristics of different materials considered for the walls.

Parameter	Body	Polyurethane	Glass Fiber Reinforced Polymer (GRFP)
Heat transfer transmittance, λ (W m^{-1} K^{-1})	60	0.024	0.64
Width, s (m)	0.005	0.064	0.002
Density, ρ (kg m^{-3})	2700	40	1800
Specific heat capacity, c (J kg^{-1} K^{-1})	900	1400	1255

Table A3 shows the nominal characteristics of the three photovoltaic panels simulated in the energy model.

Table A3. Characteristics of each type of photovoltaic panel simulated within the energy model.

Parameter	Type A	Type B	Type C
Technology	HJT	Monocrystalline	Monocrystalline
Peak power [W]	120	108	52
V_{oc} [V]	17.3	15.3	10.9
V_{mp} [V]	14	12.6	9.1
i_{mp} [A]	8.6	8.6	5.7
i_{sc} [A]	9	9	6
Dimensions [mm]	1046 × 683	1046 × 683	1109 × 293
Weight [kg]	1.7	1.7	0.8

The size of the inverter was chosen according to the peak load. Its main characteristics are presented in Table A4.

Table A4. Inverter characteristics.

Parameter	Value
Nominal power [VA/W]	3000/3000
Voltage [VAC]	230
AC Voltage regulation (battery mode) [VAC]	230 ± 5% 170–280 (For Personal Computers) 280 (For Home Appliances)
Peak power [VA]	6000
Efficiency peak [/]	90% to 93%
Transfer time [ms]	10 (For Personal Computers) 20 (For Home Appliances)
Waveshape	PURE WAVE
Battery/charge voltage [VDC]	24/27
Overcharge protection [VDC]	33
Type of charge controller	MPPT
Maximum capacity PV [W]	1500
Maximum PV array open-circuit voltage [VDC]	145
PV Array MPPT Voltage Range [VDC]	30 to 115
Maximum charge current: solar and AC/rest [A]	60/120
Relative humidity	5% to 95%
Operating/storage temperature [°C]	−10 to 50/−15 to 60

Moreover, 95% and 90% efficiency have been assumed for the DC-DC and DC-AC conversions, respectively. Therefore, a small percentage of losses (10%) caused by the continuous DC-AC conversion is added to the net electrical power required by the refrigeration unit in monthly operation and the losses in the wiring. The remaining significant losses (about 30%) are due to the conversion between DC-AC current, including the power factor ($\cos\varphi$ of 0.7).

Appendix B.

Table A5 summarizes the equations regarding the heat transfer mechanisms considered in the thermal model.

Table A5. Heat transfer in the refrigerated van.

Type of Heat Transfer	Equation
Convective between the walls' external surface and the external air [34]	$\dot{Q}_{e-w} = h_e S_e [T_{amb} - T_{w-e}(x=0)]$
Convective between the walls' external surface and the air inside the driver's cabin [34]	$\dot{Q}_{c-w} = h_c S_c [T_c - T_{w-c}(x=0)]$
Incident solar radiation [34]	$\dot{Q}_{rad} = \sum\limits_{i=1}^{4} \alpha_B G_i S_i$
Radiative with the celestial vault (the vehicle is considered a small convex object placed inside a cavity) [34]	$\dot{Q}_{w-sky} = \sigma \varepsilon_B S_{roof} \left[T_{sky}^4 - T_{w-ext}(x=0)^4 \right]$

Table A5. *Cont.*

Type of Heat Transfer	Equation
Convective between the internal air and the surface of the inner wall bordering the outside	$\dot{Q}_{in-w} = h_{in-w}S_{in-e}[T_{w-e}(x = s_{wall}) - T_{in}]$
Convective between the internal air and the walls' inner surface bordering the driver's cabin	$\dot{Q}_{i-c} = h_{in-c}S_{in-c}[T_{w-c}(x = s_{wall}) - T_{in}]$
Internal due to the auxiliaries	$\dot{Q}_{aux}$
Door opening ($\neq 0$ only in the goods loading/unloading phases, known duration) [35]	$\dot{Q}_{door} = \dot{m}_a(j_{a,0} - j_{a,in})$ where, $\dot{m}_a = \left[C_{inf}S_{door}\sqrt{H}\left(\frac{\rho_{in}-\rho_e}{2}\right)^{0.5} \left[\frac{2}{1+\left(\frac{\rho_{in}}{\rho_e}\right)^{\frac{1}{3}}}\right]\right]^{\frac{3}{2}} \left(\frac{\rho_{in}+\rho_e}{2}\right)$
Defrost system, given by electrical resistances ($\neq 0$ only during activation, known duration)	$\dot{Q}_{defrost} = 867\ W$
Cooling capacity of the refrigeration system	$\dot{Q}_{RU}$

The Fourier equation for unsteady 1D conduction is solved for the exchange with the ambient and the driver's cabin, assuming the cold room to a parallelepiped, Equation (A1).

$$\rho c \frac{\partial T_w}{\partial t} = \lambda \frac{\partial^2 T_w}{\partial x^2}. \tag{A1}$$

The boundary conditions assumed for this model are shown in Table A6.

Table A6. Boundary conditions.

Condition	Equation
With the ambient	$-\lambda \frac{\partial T_{w-e}}{\partial x}\Big|_{x=0} = h_e[T_{amb} - T_{w-e}(x = 0)] + \frac{\dot{Q}_{rad}+\dot{Q}_{w-sky}}{S_e}$
With the cabin	$-\lambda \frac{\partial T_{w-c}}{\partial x}\Big|_{x=0} = h_c[T_c - T_{w-c}(x = 0)]$
With the internal air (wall that exchanges with the ambient)	$-\lambda \frac{\partial T_{w-e}}{\partial x}\Big|_{x=s_{wall}} = h_{in}[T_{w-e}(x = s_{wall}) - T_{in}]$
With the internal air (wall that exchanges with the driver's cabin)	$-\lambda \frac{\partial T_{w-c}}{\partial x}\Big|_{x=s_{wall}} = h_{in}[T_{w-c}(x = s_{wall}) - T_{in}]$
Between two adjacent layers of the stratigraphy (*i* and *j*)	$-\lambda_i \frac{\partial T_w}{\partial x}\Big|_{x=s_i^-} = -\lambda_j \frac{\partial T_w}{\partial x}\Big|_{x=s_i^+}$

The presence of the panels is modeled by a thermal energy balance with lumped parameters, Equation (A2).

$$m_{PV}c_{PV}\frac{\partial T_{PV}}{\partial t} = \dot{Q}_{rad,PV} + h_e S_{roof}(T_{amb} - T_{PV}) + h_{AG}S_{roof}(T_{AG} - T_{PV}) + \dot{Q}_{AG}, \tag{A2}$$

where m_{PV} and c_{PV} are the mass and the specific heat of the panel, T_{PV} is the panel temperature, assumed as constant, h_e is the convective heat exchange coefficient of the ambient air, and h_{AG} of the air flowing through the interspace (*AG*, Air Gap), T_{AG} is the air temperature in the cavity, assumed as constant and equal to the external temperature T_{amb}, $\dot{Q}_{rad,PV}$ is the radiative heat exchange due to solar radiation and heat exchange with the celestial vault, as defined above, $\dot{Q}_{AG}$ is the radiative heat exchange between the lower surface of the panel and the external surface of the wall, calculated as Equation (A3) indicates.

$$\dot{Q}_{AG} = \frac{\sigma S_{roof}\left(T_{roof(0)}^4 - T_{PV}^4\right)}{\frac{1}{\alpha_{front}} + \frac{1}{\alpha_{back}} - 1}. \tag{A3}$$

The boundary condition for the roof is then determined by employing Equations (A4) and (A5).

$$-\lambda_B \frac{\partial T_w}{\partial x}\Big|_{x=0} = h_{AG}\left(T_{AG} - T_{roof}(0)\right) - \dot{q}_{AG}, \tag{A4}$$

$$\dot{q}_{AG} = \frac{\dot{Q}_{AG}}{S_{roof}}. \tag{A5}$$

The properties of the *PV* panels are defined in Table A7.

Table A7. Thermodynamic and geometrical properties of the PV panels.

Density (ρ_{PV})	Width (s_{PV})	Specific Heat Capacity (c_{PV})	Absorptivity (Front Side) (α_{front})	Absorptivity (Back Side) (α_{back})	Emissivity (ε)
2700 kg m^{-3}	0.003 m	900 J kg^{-1} K^{-1}	0.72	0.2	0.91

Appendix C.

Appendix C.1. Lithium Battery

The equation representative of the lithium battery discharge is Equation (A6) [36]. Two corrective parameters, $Corr_R$ and $Corr_K$, have been introduced, which allow considering a variation of the internal resistance as the battery charge varies (it) and the variation of the bias constant as the discharge current varies (i). These parameters are calculated using an optimization function that minimizes the mean square error between the two curves (simulated and real) at a given current value. An average and a maximum error of 0.4% and 1% are obtained.

$$V_b = \overline{V} - K \cdot \frac{Q}{Q - it} \cdot (it + i^*) - R \cdot i + A \cdot e^{-B \cdot it}, \tag{A6}$$

$$R = R_{ref}(1 + Corr_R \cdot it), \tag{A7}$$

$$K = K_{ref}(1 - Corr_K \cdot i), \tag{A8}$$

where:

- $\overline{V}$ is the constant voltage of the battery [V];
- K is the Polarization constant [V A^{-1}h^{-1}] or Polarization resistance [Ω];
- Q is the battery capacity [Ah];
- it is the actual charge of the battery [Ah];
- A is the width of the exponential area [V];
- B is the constant of time in the exponential area [Ah^{-1}];
- R is the internal resistance of the battery [Ω];
- i is the current [A];
- i^* is the filtered current [A].

For the charge instead, Equation (A9) is used. The polarization resistance varies in the charging phase model and the current direction. This ends with an increase in voltage at the end of the charging process. From a mathematical point of view, it behaves like a vertical asymptote so that the voltage will tend toward infinity at a particular state of charge.

$$V_b = \overline{V} - K \cdot \frac{Q}{Q - it} \cdot it - K \cdot \frac{Q}{it + 0.05Q} \cdot i^* - R \cdot i + A \cdot e^{-B \cdot it}. \tag{A9}$$

Note that the charging process occurs in two phases, the first phase at constant current and another phase at a constant voltage. The charger will limit the current not exceeding a voltage limit value in the constant voltage phase. This phenomenon is modeled using a current limiting function where a higher current would cause an overvoltage than the chosen limiting voltage.

Appendix C.2. Lead-Acid Battery

For the lead-acid battery discharging phase, the variability of capacitance with current according to Peukert's law has been added. The model is valid for any SOC value.

$$V_b = \overline{V} - K \cdot \frac{Q}{Q - it} \cdot it - K \cdot \frac{Q}{Q - it} \cdot i^* - R \cdot i + Exp\,(t), \tag{A10}$$

$$\dot{Q}\,(i) = \left(\frac{i}{i_{ref}}\right)^a \cdot Q_{nom}, \tag{A11}$$

$$a = \frac{\log(Q(i_2)) - \log(Q(i_1))}{\log(i_1) - \log(i_2)}, \tag{A12}$$

where:

- $Q(i)$ is the battery capacity, in Ah, at the discharge current i;
- Q_{nom} is the nominal battery capacity at a reference discharge current i_0;
- $Q(i_2)$ and $Q(i_1)$ are two different battery capacities at different discharge rates i_2 and i_1;
- $Exp\,(t)$ is the exponential voltage [V], given by:

$$Exp(t) = B \cdot |\,i\,(t)\,| \cdot (-Exp\,(t) + A \cdot u\,(t)), \tag{A13}$$

with variable $u\,(t)$ in charge ($u\,(t) = 1$) or discharge mode ($u\,(t) = 0$).

A new control phase has been added to the model for the charging phase. A map of values allows identifying the maximum currents supplied according to the SOC and the limit voltage to be charged. Therefore, currents that cause an overvoltage in the constant voltage charging phase are limited.

$$V_b = \overline{V} - K \cdot \frac{Q}{Q - it} \cdot it - K \cdot \frac{Q}{Q - 0.1\,it} \cdot i^* - R \cdot i + Exp\,(t) \tag{A14}$$

The limits imposed by the model are that: the minimum no-load battery voltage is 0 V, while the maximum battery voltage is $2\,\overline{V}$, and the minimum battery capacity is 0 Ah, while the maximum capacity is Q. Therefore, the maximum *SOC* cannot exceed 100% if the battery is overcharged.

It is possible to obtain the necessary parameters using the manual supplied with the batteries. The characteristic discharge curve is provided together with the internal resistance R of the battery. The characteristic time constant of the filtered current i^* can be obtained through experimental tests or assumed equal to 10 s (a value considered acceptable by the literature for lithium and lead-acid batteries). The calculated values for the discharge phase are also used to model the charge phase.

The state of charge (percentage of residual charge) is given by the following equation [37]:

$$SOC(t) = SOC(0) + \frac{\eta_i \int_0^t i(t)dt}{Q}. \tag{A15}$$

The efficiency η_i is the Coulombic efficiency, with a unitary value in the case of discharge and less than one in the case of charge (variable according to the type of battery).

The slow dynamics of voltage adjustment for an instantaneous step change of the current is modeled by the filtered current i^* flowing through the bias resistor:

$$\frac{i - i^*}{\tau} = \frac{di^*}{dt}, \tag{A16}$$

with τ representing the characteristic time constant of the considered battery.

The model can simulate the experimental voltage with a good approximation, with an error below 5% throughout the charging process.

Appendix C.3. Generalization of the Model

The two types of battery considered so far have been modeled considering a 12 V 100 Ah battery so that all the parameters refer to this battery size. To obtain the capacity and voltage of a generically sized battery, it is necessary to identify generalized parameters.

For a generic capacity:

$$Q_{conv} = \frac{Q_{ref}}{Q_{nom}}, \tag{A17}$$

where Q_{conv} is a conversion parameter obtained as the ratio between the reference capacity (in this case, 100 Ah) and the nominal capacity of the battery that we want to adopt.

By the same reasoning, the correction parameters and the internal resistance are:

$$Corr_R = \frac{Corr_{R,ref}}{Q_{conv}}, \tag{A18}$$

$$Corr_K = \frac{Corr_{K,ref}}{Q_{conv}}, \tag{A19}$$

$$R = R_{ref} * Q_{conv}. \tag{A20}$$

For a generic voltage:

$$V_{conv} = \frac{V_{ref}}{V_{nom}}, \tag{A21}$$

$$R = \frac{R_{ref}}{V_{conv}}. \tag{A22}$$

So, for a generic voltage and a generic capacity:

$$R = \frac{R_{ref}}{V_{conv}} * Q_{conv}. \tag{A23}$$

References

1. AssoGasMetano. Available online: https://www.assogasmetano.it/prezzo-medio-nazionale-2018/ (accessed on 6 March 2020).
2. Barth, M.; Younglove, T.; Scora, G. Development of a Heavy-Duty Diesel Modal Emissions and Fuel Consumption Model. 2005. UC Berkeley California Partners for Advanced Transportation Technology. Available online: https://escholarship.org/uc/item/67f0v3zf (accessed on 2 June 2022).
3. Blasko, V.; Bendapudi, S.; Oggianu, S.M. Solar Power Assisted Transport Refrigeration Systems, Transport Refrigeration Units and Methods for Same. U.S. Patent US20130000342A1, 3 January 2013.
4. Cenex. *Refrigerated Transport Insights-A ZERO White Paper*; Cenex: Loughborough, UK, 2021.
5. Chang, W.-Y. The State of Charge Estimating Methods for Battery: A Review. *ISRN Appl. Math.* **2013**, *2013*, 953792. [CrossRef]
6. Citarella, B.; Viscito, L.; Mochizuki, K.; Mauro, A.W. Multi-criteria (thermo-economic) optimization and environmental analysis of a food refrigeration system working with low environmental impact refrigerants. *Energy Convers. Manag.* **2022**, *253*, 115152. [CrossRef]
7. Franceschetti, A.; Honhon, D.; Van Woensel, T.; Bektaş, T.; Laporte, G. The time-dependent pollution-routing problem. *Transp. Res. Part B Methodol.* **2013**, *56*, 265–293. [CrossRef]
8. Górny, K.; Stachowiak, A.; Tyczewski, P.; Zwierzycki, W. Lubricity of selected oils in mixtures with the refrigerants R452A, R404A, and R600a. *Tribol. Int.* **2019**, *134*, 50–59. [CrossRef]
9. Infante Ferreira, C.; Kim, D.-S. Techno-economic review of solar cooling technologies based on location-specific data. *Int. J. Refrig.* **2014**, *39*, 23–37. [CrossRef]
10. ISPRA. 2019. Available online: https://www.isprambiente.gov.it/files2019/pubblicazioni/rapporti/R_303_19_gas_serra_settore_elettrico.pdf (accessed on 6 March 2020).
11. Kim, D.S.; Infante Ferreira, C.A. Solar refrigeration options–a state-of-the-art review. *Int. J. Refrig.* **2008**, *31*, 3–15. [CrossRef]
12. Ladha-Sabur, A.; Bakalis, S.; Fryer, P.J.; Lopez-Quiroga, E. Mapping energy consumption in food manufacturing. *Trends Food Sci. Technol.* **2019**, *86*, 270–280. [CrossRef]
13. Lawton, R.; Curlin, J.S.; Clark, W. *Technology Brief IIR-UN Environment Cold Chain Brief on Transport Refrigeration*; International Institute of Refrigeration (IIFIIR): Paris, Prance, 2018; Available online: https://wedocs.unep.org/bitstream/handle/20.500.11822/32571/8142Transpor_Ref_EN.pdf?sequence=1&isAllowed=y (accessed on 2 June 2022).
14. Lazzarin, R.M. Solar cooling: PV or thermal? A thermodynamic and economical analysis. *Int. J. Refrig.* **2014**, *39*, 38–47. [CrossRef]
15. Lazzarin, R.M.; Noro, M. Past, present, future of solar cooling: Technical and economical considerations. *Sol. Energy* **2018**, *172*, 2–13. [CrossRef]
16. Li, G. Comprehensive investigation of transport refrigeration life cycle climate performance. *Sustain. Energy Technol. Assess.* **2017**, *21*, 33–49. [CrossRef]

17. Mahmoudi, M.; Dehghan, M.; Haghgou, H.; Keyanpour-Rad, M. Techno-economic performance of photovoltaic-powered air-conditioning heat pumps with variable-speed and fixed-speed compression systems. *Sustain. Energy Technol. Assess.* **2021**, *45*, 101113. [CrossRef]
18. Maiorino, A.; Petruzziello, F.; Aprea, C. Refrigerated Transport: State of the Art, Technical Issues, Innovations and Challenges for Sustainability. *Energies* **2021**, *14*, 7237. [CrossRef]
19. Meneghetti, A.; Ceschia, S. Energy-efficient frozen food transports: The Refrigerated Routing Problem. *Int. J. Prod. Res.* **2020**, *58*, 4164–4181. [CrossRef]
20. Mota-Babiloni, A.; Makhnatch, P. Predictions of European refrigerants place on the market following F-gas regulation restrictions. *Int. J. Refrig.* **2021**, *127*, 101–110. [CrossRef]
21. Nasuta, D.; Srichai, R.; Zhang, M.; Martin, C.; Muehlbauer, J. Life Cycle Climate Performance Model for Transport Refrigeration/Air Conditioning Systems. *ASHRAE Trans.* **2014**, *120*, 1P–8P.
22. Njoroge, P.; Ndunya, L.S.; Kabiru, P. Hybrid Solar-Wind Power System for Truck Refrigeration. In Proceedings of the 2018 IEEE PES/IAS PowerAfrica, Cape Town, South Africa, 28–29 June 2018; pp. 1–9.
23. De Novaes Pires Leite, G.; Weschenfelder, F.; Araújo, A.M.; Villa Ochoa, Á.A.; da Franca Prestrelo Neto, N.; Kraj, A. An economic analysis of the integration between air-conditioning and solar photovoltaic systems. *Energy Convers. Manag.* **2019**, *185*, 836–849. [CrossRef]
24. Rai, A.; Tassou, S.A. Energy demand and environmental impacts of alternative food transport refrigeration systems. *Energy Procedia* **2017**, *123*, 113–120. [CrossRef]
25. Reda, F.; Paiho, S.; Pasonen, R.; Helm, M.; Menhart, F.; Schex, R.; Laitinen, A. Comparison of solar assisted heat pump solutions for office building applications in Northern climate. *Renew. Energy* **2020**, *147*, 1392–1417. [CrossRef]
26. Riva, C.; Roumpedakis, T.C.; Kallis, G.; Rocco, M.V.; Karellas, S. Life cycle analysis of a photovoltaic driven reversible heat pump. *Energy Build.* **2021**, *240*, 110894. [CrossRef]
27. Salilih, E.M.; Birhane, Y.T. Modelling and performance analysis of directly coupled vapor compression solar refrigeration system. *Sol. Energy* **2019**, *190*, 228–238. [CrossRef]
28. Sarbu, I.; Sebarchievici, C. Review of solar refrigeration and cooling systems. *Energy Build.* **2013**, *67*, 286–297. [CrossRef]
29. Sovacool, B.K.; Bazilian, M.; Griffiths, S.; Kim, J.; Foley, A.; Rooney, D. Decarbonizing the food and beverages industry: A critical and systematic review of developments, sociotechnical systems and policy options. *Renew. Sustain. Energy Rev.* **2021**, *143*, 110856. [CrossRef]
30. Stoecker, W.F. *Industrial Refrigeration Handbook*; McGraw-Hill Education: New York, NY, USA, 1998.
31. Su, P.; Ji, J.; Cai, J.; Gao, Y.; Han, K. Dynamic simulation and experimental study of a variable speed photovoltaic DC refrigerator. *Renew. Energy* **2020**, *152*, 155–164. [CrossRef]
32. Tassou, S.A.; De-Lille, G.; Ge, Y.T. Food transport refrigeration—Approaches to reduce energy consumption and environmental impacts of road transport. *Appl. Therm. Eng.* **2009**, *29*, 1467–1477. [CrossRef]
33. Torregrosa-Jaime, B.; Bjurling, F.; Corberán, J.M.; Di Sciullo, F.; Payá, J. Transient thermal model of a vehicle's cabin validated under variable ambient conditions. *Appl. Therm. Eng.* **2015**, *75*, 45–53. [CrossRef]
34. Tremblay, O.; Dessaint, L.A. Experimental validation of a battery dynamic model for EV applications. *World Electr. Veh. J.* **2009**, *3*, 289–298. [CrossRef]
35. UNECE. *Climate Change and Sustainable Transport*; UNECE: Geneva, Switzerland, 2021.
36. Wu, X.; Hu, S.; Mo, S. Carbon footprint model for evaluating the global warming impact of food transport refrigeration systems. *J. Clean. Prod.* **2013**, *54*, 115–124. [CrossRef]
37. Yang, Z.; Tate, J.E.; Morganti, E.; Shepherd, S.P. Real-world CO_2 and NOX emissions from refrigerated vans. *Sci. Total Environ.* **2021**, *763*, 142974. [CrossRef]